



## Suppression of molecular field by lattice contraction in face-centered-cubic $R\text{Ni}_4\text{Cd}$ ( $R = \text{Ce}, \text{Nd}, \text{Sm}, \text{and Gd-Tm}$ )

Jeonghun Lee  and Eundeok Mun 

Department of Physics, Simon Fraser University, 8888 University Drive, Burnaby, British Columbia, Canada V5A 1S6



(Received 17 August 2023; revised 30 October 2023; accepted 30 October 2023; published 13 November 2023)

Single crystals of  $R\text{Ni}_4\text{Cd}$  ( $R = \text{Ce}, \text{Nd}, \text{Sm}, \text{and Gd-Tm}$ ) are grown by Cd flux and their physical properties are investigated by means of x-ray diffraction, magnetization, electrical resistivity, and specific heat measurements. Except for  $R = \text{Ce}$ , the unit cell volume of  $R\text{Ni}_4\text{Cd}$  follows a lanthanide contraction, implying a  $3+$  valence state of rare-earth ions in this series. At high temperatures, magnetic susceptibility curves for  $R = \text{Nd}$  and  $\text{Gd-Tm}$  follow the Curie-Weiss behavior. The obtained Curie-Weiss temperature ( $\theta_p$ ) for  $R = \text{Gd-Tm}$  is small and negative. The temperature dependence of the electrical resistivity shows a metallic behavior for all  $R\text{Ni}_4\text{Cd}$  compounds. Of the thermodynamic and transport property measurements, only  $\text{GdNi}_4\text{Cd}$  indicates an antiferromagnetic ordering below  $T_N = 4.5$  K, while the remaining compounds show no signature of magnetic transition down to 1.8 K. The Ruderman-Kittel-Kasuya-Yosida (RKKY) exchange mechanism is examined for its relevance to  $T_N$  and  $\theta_p$  of isostructural metallic  $RT_4X$  ( $R = \text{Gd-Tm}$ ,  $T = \text{Cu}$  and  $\text{Ni}$ , and  $X = \text{Cd}, \text{In}, \text{Mg}, \text{Pd}, \text{Ag}, \text{and Au}$ ) compounds. Although the variation in  $\theta_p$  can be qualitatively explained by the RKKY sum, the values of  $\theta_p$  in this family are highly dependent on their lattice parameter. Unlike the  $RCu_4X$ , the strength of the exchange interaction between molecular fields produced by rare-earth planes is strongly suppressed by the lattice contraction in  $R\text{Ni}_4X$  compounds.

DOI: [10.1103/PhysRevB.108.184409](https://doi.org/10.1103/PhysRevB.108.184409)

### I. INTRODUCTION

The  $RT_4X$  ( $R = \text{rare-earth}$ ,  $T = \text{Cu}$  and  $\text{Ni}$ , and  $X = \text{Cd}, \text{In}, \text{Mg}, \text{Pd}, \text{Ag}, \text{and Au}$ ) compounds adopt a  $\text{MgCu}_4\text{Sn}$ -type structure ( $F\bar{4}3m$ , No. 216) in which rare-earth atoms occupy a face-centered-cubic (fcc) lattice forming a network of edge-sharing tetrahedra [1–7]. Since all three ( $R$ ,  $T$ , and  $X$ ) positions can be substituted without changing the underlying crystal structure, this family of materials is well suited to study the evolution of physical properties and their relationships through chemical substitution. Within this family of materials, the low-carrier-density semimetallic  $RCu_4\text{In}$  compounds exhibit large values of the magnetic frustration parameter ( $f \sim 10$ ), which is defined as the ratio between the absolute value of the Curie-Weiss temperature  $|\theta_p|$  and the magnetic ordering temperature  $T_N$ , i.e.,  $f = |\theta_p|/T_N$ . It has been suggested that short-range superexchange interaction between rare earths results in a low magnetic ordering temperature, giving rise to a large value of  $f$  ( $T_N \ll |\theta_p|$ ) [3,8]. Conversely, the good metallic  $RCu_4\text{Cd}$  compounds exhibit a much smaller  $f$  value [3]. When the carrier density is increased, the frustration parameter becomes smaller ( $f \sim 1$ ) [3]. The  $\text{GdCu}_4\text{In}_{1-x}\text{Cd}_x$  system reveals a systematic change in electrical resistivity from a semiconductorlike behavior ( $x = 0$ ) to a metallic one ( $x = 1$ ), resulting in an increase of  $T_N$  from 5.5 to 38 K and a decrease of  $\theta_p$  from  $-52$  to  $-72$  K, and thus changing  $f$  from  $\sim 10$  to  $\sim 2$  [3]. In addition, replacing Cu with Ni in  $\text{Gd}(\text{Cu}_{1-x}\text{Ni}_x)_4\text{In}$  makes the system a good metal, changing  $\theta_p$  from a large negative value to a small positive one, while maintaining  $T_N$  near 5 K [9].

The series  $RT_4X$  ( $R = \text{heavy rare earth}$ ) provides a way to compare the magnetism of highly localized  $4f$  elements that share a similar crystal field environment. To gain insight into the evolution of  $\theta_p$  in this series,  $\theta_p$  values are plotted in Fig. 1 as a function of the lattice parameter for all isostructural  $RT_4X$  ( $R = \text{Gd-Tm}$ ) compounds. For the antiferromagnetic (AFM) compounds,  $\theta_p$  weakly depends on the lattice parameter below  $\sim 7.10$  Å, while  $\theta_p$  rapidly decreases above  $\sim 7.15$  Å toward a very large negative value. For the ferromagnetic  $RCu_4\text{Pd}$  compounds,  $\theta_p$  deviate from this trend. The effective moment values of these compounds, obtained from magnetic susceptibility measurements, are consistent with the theoretical values of free rare-earth ions, indicating a localized moment on  $R$  and no moment on  $T$  and  $X$ . The lattice parameter of  $\text{GdNi}_4\text{Cd}$ , obtained from the previously studied polycrystalline sample [1], locates a value near 7.06 Å, where  $\theta_p$  starts to saturate close to zero as the lattice parameter decreases. When the Gd ions are replaced by smaller rare earths, it would be interesting to see whether  $\theta_p$  of  $R\text{Ni}_4\text{Cd}$  follows the same trend as the AFM  $RT_4X$ . Except for  $R = \text{Yb}$  and  $\text{Y}$  [11], the physical properties of  $R\text{Ni}_4\text{Cd}$  compounds have not been previously reported. Thus, we grew single crystals of  $R\text{Ni}_4\text{Cd}$  ( $R = \text{Ce}, \text{Nd}, \text{Sm}, \text{Gd-Tm}$ ) and report their physical properties, characterized by powder x-ray diffraction, magnetization, resistivity, and specific heat measurements. To qualitatively understand the variations of  $\theta_p$  in the isostructural  $RT_4X$  ( $R = \text{Gd-Tm}$ ,  $T = \text{Cu}$  and  $\text{Ni}$ , and  $X = \text{Cd}, \text{In}, \text{Mg}, \text{Pd}, \text{Ag}, \text{and Au}$ ) compounds, we compare all observed values of  $\theta_p$  in the  $RT_4X$  series and explain the variations using Ruderman-Kittel-Kasuya-Yosida (RKKY) theory.

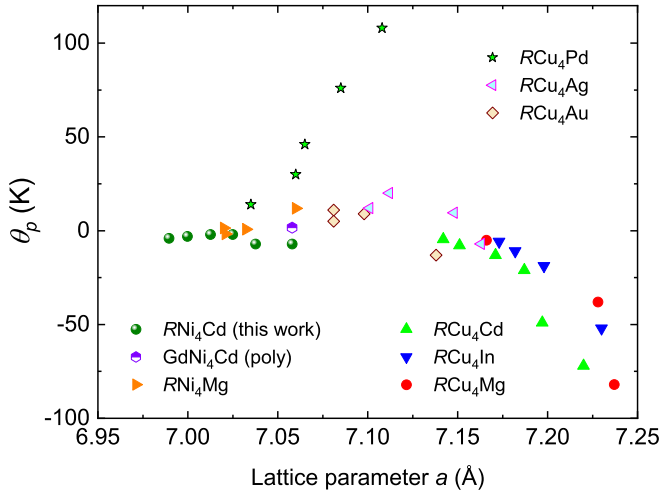


FIG. 1.  $\theta_p$  of  $RT_4X$  ( $R = \text{Gd-Tm}$ ,  $T = \text{Cu}$  and  $\text{Ni}$ , and  $X = \text{Cd}$ ,  $\text{In}$ ,  $\text{Mg}$ ,  $\text{Pd}$ ,  $\text{Ag}$ , and  $\text{Au}$ ) as a function of lattice parameter  $a$ . Except  $R\text{Ni}_4\text{Cd}$ ,  $\theta_p$  and  $a$  values are taken from Ref. [10].

## II. EXPERIMENTS

Single crystals of  $R\text{Ni}_4\text{Cd}$  ( $R = \text{Ce}$ ,  $\text{Nd}$ ,  $\text{Sm}$ ,  $\text{Gd-Tm}$ ) were grown by Cd flux [11]. High-purity rare-earth, Ni, and Cd were loaded into an alumina crucible in the ratio of 1 : 4 : 25 and sealed into an amorphous silica tube. The ampoule was heated to 1050 °C and slowly cooled down to 750 °C at the rate of 2 °C/hr. Note that an attempt to grow single crystals for  $R = \text{La}$  and  $\text{Pr}$  was unsuccessful using this method. Powder x-ray diffraction (XRD) patterns of crushed  $R\text{Ni}_4\text{Cd}$  single crystals were taken at room temperature in a Rigaku MiniFlex diffractometer.

Analysis, via FULLPROF software, of powder XRD patterns confirms that all  $R\text{Ni}_4\text{Cd}$  samples crystallize into the  $\text{MgCu}_4\text{Sn}$ -type structure ( $F\bar{4}3m$ , No. 216), which is an ordered variant of the  $\text{AuBe}_5$ -type structure [12]. The powder XRD of  $\text{DyNi}_4\text{Cd}$  is shown in Fig. 2(a), where the open symbol and red line are the observed and calculated XRD profiles, respectively. No other phases have been detected except minor Cd. The crystal structure is shown in the inset of Fig. 2(a) [1], where Ni atoms form a network of corner-sharing tetrahedra (Wyckoff 16e site) which leave cavities; these are filled in an orderly way by Cd (Wyckoff 4a site) and  $R$  (Wyckoff 4c site). The cubic point symmetry ( $T_d$ ) on rare-earth ions minimizes magnetic anisotropy. Each Cd and  $R$  forms fcc sublattices, making a network of edge-sharing tetrahedra. The obtained lattice parameters (red solid circle) of  $R\text{Ni}_4\text{Cd}$  single crystals, plotted in Fig. 2(b), are in good agreement with a previous polycrystalline sample (open star) study [1]. Except Ce, the lattice parameter of  $R\text{Ni}_4\text{Cd}$  follows lanthanide contraction, indicating a 3+ valence state of rare-earth ions. For  $\text{CeNi}_4\text{Cd}$ , a deviation from the lanthanide contraction implies a 4+ valence state of Ce ions.

All physical property measurements were performed using polished single crystal samples. The dc magnetization, for temperatures ranging from 1.8 to 300 K and magnetic field up to 70 kOe applied along the [111] crystallographic direction, was collected in a Quantum Design (QD) Magnetic Property Measurement System (MPMS). The standard four-probe

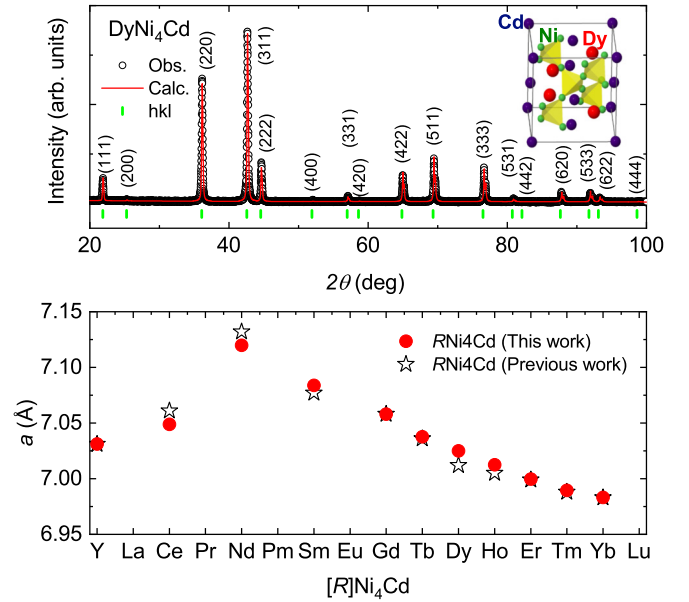


FIG. 2. (top panel) Observed (open symbol) and calculated (red line) powder x-ray diffraction patterns of a crushed single crystal from  $\text{DyNi}_4\text{Cd}$ . (bottom panel) Lattice parameters of  $R\text{Ni}_4\text{Cd}$  ( $R = \text{Ce}$ ,  $\text{Nd}$ ,  $\text{Sm}$ ,  $\text{Gd-Tm}$ ) obtained from this work (single crystals) and the previous single crystals for  $R = \text{Y}$  and  $\text{Yb}$  [11] and polycrystalline samples [1].

resistivity measurements were performed from 300 to 1.8 K in a QD Physical Property Measurement Systems (PPMS). Specific heat was measured by the relaxation method down to  $T = 1.8$  K in a QD PPMS.

## III. RESULTS

### A. Light rare earth ( $R = \text{Ce}$ , $\text{Nd}$ , $\text{Sm}$ )

Figures 3(a) and 3(b) show magnetization measurements as a function of temperature and magnetic field, respectively, for  $R = \text{Ce}$ ,  $\text{Nd}$ , and  $\text{Sm}$ . Note that we use cgs units for the magnetization plots. The magnetic susceptibility,  $\chi(T) = M/H$ , of  $\text{CeNi}_4\text{Cd}$  does not follow the Curie-Weiss (CW) law,  $\chi(T) = C/(T - \theta_p)$ , where  $\chi(T)$  weakly depends on the temperature at high temperatures. The 4+ valence state of Ce ions can be clearly deduced from the deviation of CW law in magnetic susceptibility, the departure of the lanthanide contraction in the lattice parameter, and the small residual magnetization at  $T = 1.8$  K. For  $R = \text{Nd}$ , the inverse magnetic susceptibility  $H/M$  is linear in temperature above  $\sim 50$  K, where the estimated effective moment,  $\mu_{\text{eff}} = 4.24 \mu_B/\text{Nd}$ , is somewhat larger than the theoretical value of  $3.62 \mu_B/\text{Nd}$ . As shown in Fig. 3(b), the magnetization value at 1.8 K and 70 kOe is  $2.3 \mu_B/\text{mol}_{\text{Nd}}$ , which is smaller than the fully saturated moment value  $gJ = 36/11$ , probably due to the crystalline electric field effects. For  $R = \text{Sm}$ , it is well known that the nonlinearity in the plot of inverse magnetic susceptibility arises because the first excited state of the Hund's rule multiplet ( $J = 7/2$ ) is very close to the ground state ( $J = 5/2$ ). For this reason, the inverse magnetic susceptibility for  $R = \text{Sm}$  is fitted only at low temperatures by the modified CW formula  $\chi(T) = \chi_0 + C/(T - \theta_p)$  to estimate its effective moment

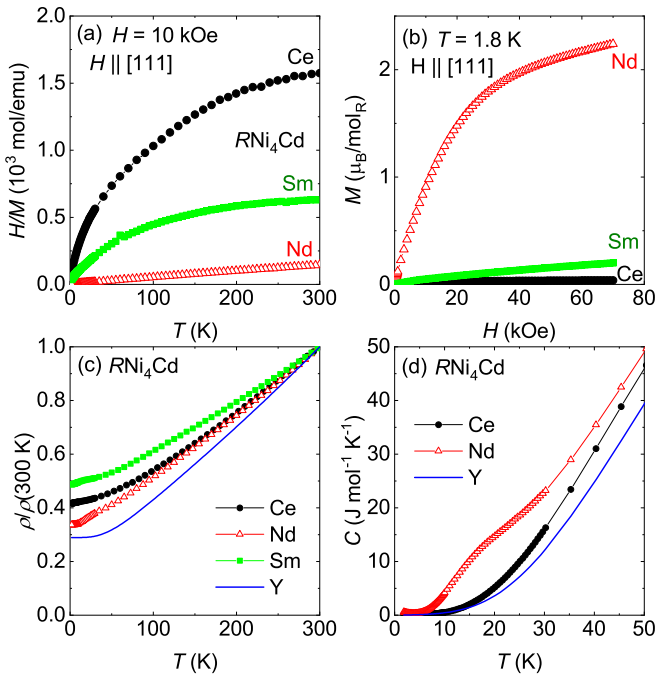


FIG. 3. Magnetization measurements of  $R\text{Ni}_4\text{Cd}$  for  $R = \text{Ce}, \text{Nd}$ , and  $\text{Sm}$ . (a) Inverse magnetic susceptibility at  $H = 10 \text{ kOe}$ . (b) Isothermal magnetization at  $T = 1.8 \text{ K}$ . (c)  $\rho(T)/\rho(300 \text{ K})$  vs  $T$ . (d) Specific heat at low temperatures.

and  $\theta_p$ . The estimated effective moment  $\mu_{\text{eff}} \sim 0.95 \mu_B/\text{Sm}$  with the Hund's rule ground state  $J = 5/2$  is slightly larger than the theoretical value of  $0.84 \mu_B/\text{Sm}$ . The isothermal magnetization at  $1.8 \text{ K}$  and  $70 \text{ kOe}$  is smaller than its  $gJ$  value, as shown in Fig. 3(b). Electrical resistivity curves normalized at  $300 \text{ K}$ ,  $\rho(T)/\rho(300 \text{ K})$ , of  $R\text{Ni}_4\text{Cd}$  ( $R = \text{Ce}, \text{Nd}, \text{Sm}$ , and  $\text{Y}$ ) are plotted in Fig. 3(c), where the resistivity curves indicate a metallic behavior. The low-temperature specific heat of  $R\text{Ni}_4\text{Cd}$  ( $R = \text{Ce}, \text{Nd}$ , and  $\text{Y}$ ) clearly confirms there are no phase transitions in these compounds, as shown in Fig. 3(d). The specific heat curve of  $\text{NdNi}_4\text{Cd}$  indicates a broad hump around  $20 \text{ K}$ , which is probably due to the crystalline electric field (CEF) effect. The electrical resistivity and specific heat of  $\text{YNi}_4\text{Cd}$  are consistent with an earlier report [11].

### B. Heavy rare earth ( $R = \text{Gd-Tm}$ )

The  $H/M$  curves of  $R\text{Ni}_4\text{Cd}$  ( $R = \text{Gd-Tm}$ ), measured at  $H = 10 \text{ kOe}$  along  $H \parallel [111]$ , are plotted in Fig. 4(a). In contrast to the light rare-earth compounds,  $H/M$  curves of heavy rare-earth compounds follow the Curie-Weiss behavior at high temperatures. Thus,  $\mu_{\text{eff}}$  and  $\theta_p$  are estimated by fitting the curves with the CW formula from  $150$  to  $300 \text{ K}$ . The obtained results are summarized in Table I. The values of  $\mu_{\text{eff}}$  are found to be consistent with that of respective trivalent rare-earth ions.

The small and negative values of  $\theta_p$  suggest a weak antiferromagnetic nature of the exchange interaction between rare-earth ions. The obtained  $\theta_p$  deviates from the de Gennes factor (dG) scaling [13]. At low temperatures, only  $\text{GdNi}_4\text{Cd}$  shows a peak at  $4.5 \text{ K}$  in the magnetic susceptibility as a signature of magnetic ordering. For the rest of the rare

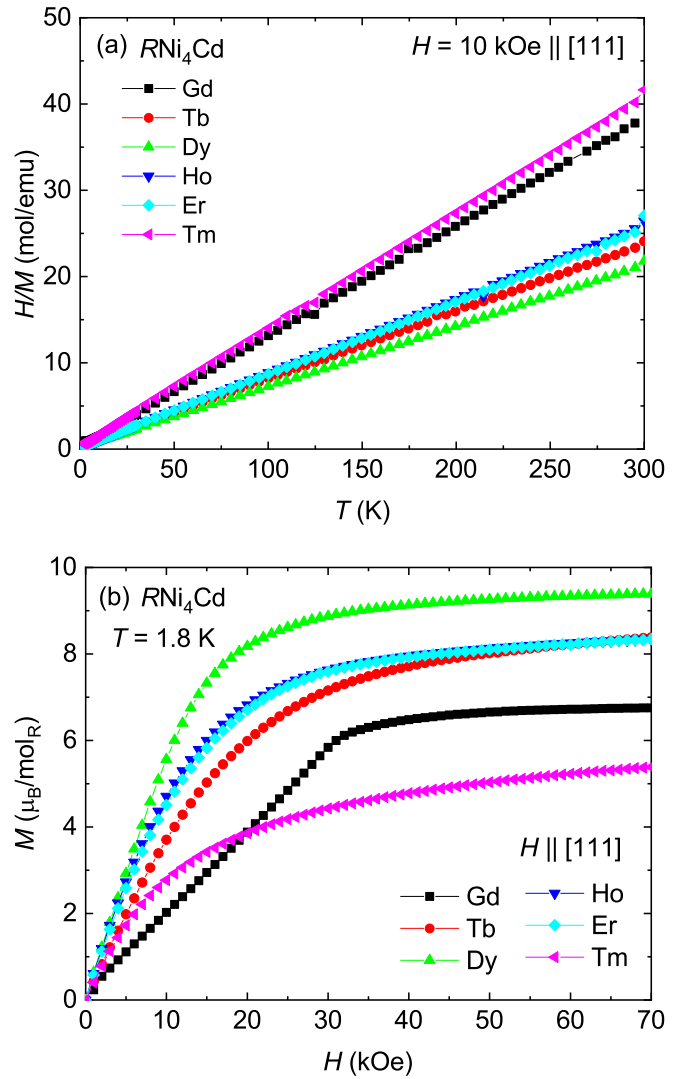


FIG. 4. Magnetic properties of  $R\text{Ni}_4\text{Cd}$  for  $R = \text{Gd-Tm}$ . (a) Inverse magnetic susceptibility at  $H = 10 \text{ kOe}$ . (b) Isothermal magnetization at  $T = 1.8 \text{ K}$ .

TABLE I. A summary of magnetic properties of  $R\text{Ni}_4\text{Cd}$  obtained from magnetic susceptibility measurements.  $M$  (70 kOe): absolute value of magnetization in  $\mu_B/R$  at  $H = 70 \text{ kOe}$  and  $T = 1.8 \text{ K}$ .  $\mu_{\text{eff}}$ : effective moment in  $\mu_B/R$  obtained from Curie-Weiss (CW) fit and modified Curie-Weiss (MCW) fit. Value inside the parentheses is the theoretical value for trivalent  $R$ .  $\Theta_p$ : paramagnetic Curie-Weiss temperature in K.  $T_N$ : magnetic ordering temperature in K.

$R$	$M$ (70 kOe)	$\mu_{\text{eff}}$	$\Theta_p$	$T_N$	Fit method
Ce	0.04 (2.1)	N/A (2.54)	N/A		N/A
Nd	2.24 (3.2)	4.24 (3.62)	-27		CW
Sm	0.20 (0.7)	0.95 (0.84)	3		MCW
Gd	6.76 (7)	7.93 (7.94)	-7	4.5	CW
Tb	8.39 (9)	10.17 (9.72)	-7		CW
Dy	9.39 (10)	10.63 (10.63)	-2		CW
Ho	8.34 (10)	9.66 (10.60)	-2		CW
Er	8.34 (9)	9.75 (9.59)	-3		CW
Tm	5.38 (7)	7.71 (7.51)	-4		CW

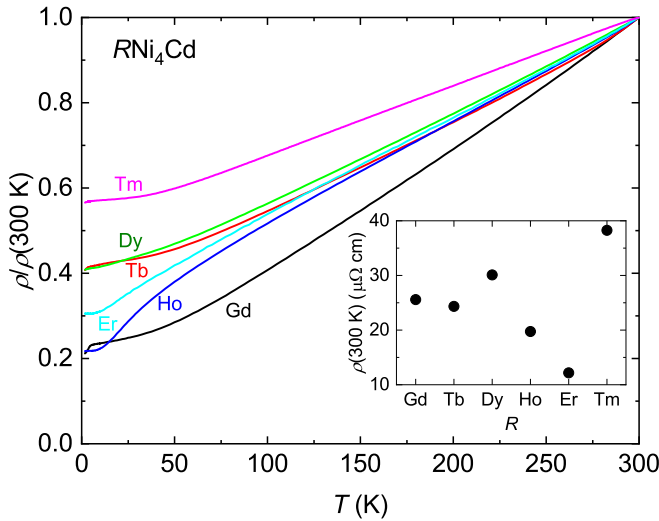


FIG. 5. Normalized  $\rho/\rho(300\text{ K})$  of  $R\text{Ni}_4\text{Cd}$  in zero field. Inset: The absolute value of resistivity at 300 K.

earths, the magnetic susceptibility measurement at  $H = 1$  kOe indicates no magnetic transition down to 1.8 K. Note that  $\text{YbNi}_4\text{Cd}$  undergoes an antiferromagnetic ordering below  $T_N = 0.97\text{ K}$  [11]. The isothermal magnetization for  $R = \text{Gd-Tm}$ , plotted in Fig. 4(b), linearly increases with the field and indicates a tendency to saturate above 20 kOe. The magnetization values at 70 kOe are somewhat smaller than the theoretical  $gJ$  values.

The electrical resistivity curves,  $\rho(T)/\rho(300\text{ K})$ , for  $R = \text{Gd-Tm}$  are plotted in Fig. 5. The  $\rho(T)$  for all compounds follows a metallic behavior. The absolute value of the resistivity at 300 K is shown in the inset. The  $\rho(300\text{ K})$  values can vary between samples and are largely dependent on the geometry error. Unlike the  $R\text{Cu}_4\text{In}$  series, the  $R\text{Ni}_4\text{Cd}$  series has consistently low resistivity values for all measured temperatures, which is similar to that of  $R\text{Cu}_4\text{Cd}$  [3].

The temperature dependence of the specific heat,  $C_p$ , curves for  $R = \text{Gd-Tm}$  and Y are shown in Fig. 6. Among  $R\text{Ni}_4\text{Cd}$  compounds, only  $\text{GdNi}_4\text{Cd}$  shows a clear  $\lambda$ -like peak at 4.5 K, which is the onset of the antiferromagnetic ordering.  $C_p$  for  $R = \text{Tb-Er}$  indicates an upturn at low temperatures, where the rise in specific heat as the temperature decreases may suggest a possible magnetic ordering below 1.8 K. It is necessary to measure specific heat below 1.8 K to confirm whether magnetic ordering exists. The specific heat for  $R = \text{Tm}$  shows a broad maximum around 3 K (more clearly seen in the inset), which can be related to a Schottky anomaly due to low-lying CEF levels. The magnetic part of the specific heat ( $C_m$ ) of  $R\text{Ni}_4\text{Cd}$  ( $R = \text{Gd-Tm}$ ) is estimated by subtracting the specific heat of  $\text{YNi}_4\text{Cd}$  and is plotted in the inset of Fig. 6. The  $C_m$  curves for  $R = \text{Tb-Tm}$  indicate broad maxima at high temperatures, which correspond to the Schottky contributions, as the  $R^{3+}$  ions are influenced by the CEF.

### C. $\text{GdNi}_4\text{Cd}$

Since  $\text{GdNi}_4\text{Cd}$  is the only  $R\text{Ni}_4\text{Cd}$  single crystal to exhibit a magnetic ordering at 4.5 K, the magnetic properties of this compound are more thoroughly investigated. Magnetic

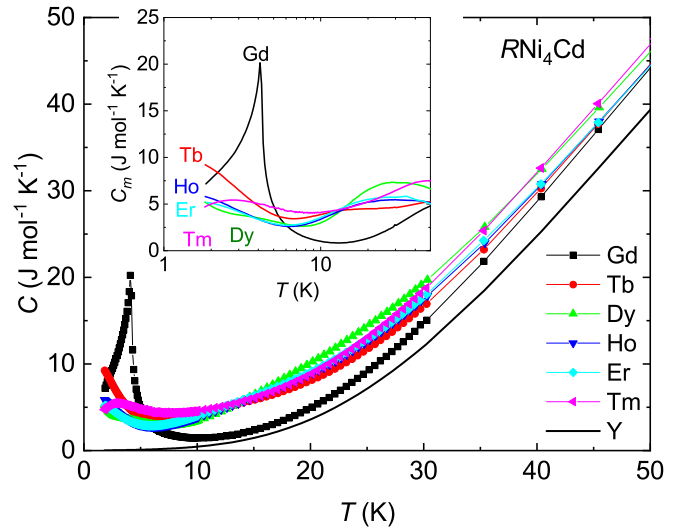


FIG. 6. Specific heat of  $R\text{Ni}_4\text{Cd}$  below 50 K. Inset: The magnetic part of the specific heat.

susceptibility of  $\text{GdNi}_4\text{Cd}$  at  $H = 1$  kOe shows a peak at 4.1 K and a hump near  $T \sim 3.0\text{ K}$ , as shown in Fig. 7(a). The resistivity in zero field is plotted alongside susceptibility, showing a sharp drop below 4.5 K, probably due to the loss of spin-disorder scattering. The observed ordering temperature in our single crystal sample is consistent with the previously reported polycrystalline sample [1]. However, a ferromagnetic ordering at  $T \sim 32\text{ K}$ , observed in the previous polycrystalline sample due to the binary  $\text{GdNi}_5$  inclusion [1], is not detected in our single crystal sample.

The magnetic specific heat  $C_m$  in zero field also shows a clear  $\lambda$ -like transition at 4.5 K, as shown in Fig. 7(b). The

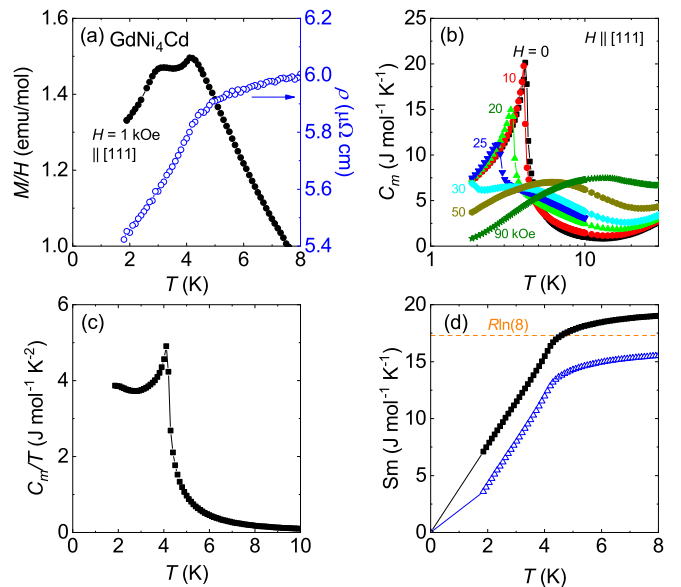


FIG. 7. Low-temperature magnetic susceptibility, specific heat, and resistivity of  $\text{GdNi}_4\text{Cd}$ . (a) Magnetic susceptibility at  $H = 1$  kOe (left axis) and resistivity in zero field (right axis). (b) Magnetic specific heat at various magnetic fields. (c)  $C_m/T$  vs  $T$  in zero field. (d) Estimated  $S_m$  in zero field. See details in the text.

magnetic ordering can be suppressed below 1.8 K by an external magnetic field less than  $\sim 50$  kOe. A broad maximum in  $C_m$  is developed at  $T \sim 3.5$  K at  $H = 30$  kOe and this maximum moves to a higher temperature as the magnetic field increases, which is probably due to the Zeeman splitting of  $S = 7/2$  energy level. The magnetic specific heat divided by temperature,  $C_m/T$ , is plotted in Fig. 7(c).  $C_m/T$  does not go to zero below the magnetic ordering temperature, showing a slight upturn below 2.7 K. Below the magnetic ordering temperature, an anomalous temperature dependence of the specific heat typically occurs in Gd-based compounds arising from the broken degeneracy of the Gd ground state [14]. Note that the nuclear Schottky anomaly is observed near  $T = 0.25$  K in  $\text{HoCu}_4\text{In}$  and  $\text{HoCu}_4\text{Cd}$  [15]. We believe that the upturn just below  $T_N$  in  $C_m/T$  of  $\text{GdNi}_4\text{Cd}$  does not originate from the nuclear spin, but from the contribution of the Schottky anomaly arising from broken degeneracy of the ground state  $J$ . Since  $C_m/T$  does not go to zero, the magnetic entropy ( $S_m$ ) is estimated by two scenarios. First,  $C_m/T$  below 1.8 K is linearly extrapolated to zero temperature with the value of  $3.8 \text{ J}/(\text{mol K}^2)$ , which may reflect the upper limit of  $S_m$ .  $S_m$  in this limit (solid symbols) almost reaches the full  $R \ln(8)$  entropy at  $T_N$ , as shown in Fig. 7(d). Second,  $C_p$  must be zero at zero temperature; thus we assume  $C_m/T = 0$  at 0 K, which can be considered as the lower limit (underestimate of the magnetic entropy). The estimated  $S_m$  in this limit (open symbol) recovers 70% of  $R \ln(8)$  by  $T_N$ . It has been observed in this family of materials that the  $S_m$  value at  $T_N$  is 86% of  $R \ln(8)$  for  $\text{GdCu}_4\text{Cd}$  [3] and 67% of  $R \ln(8)$  for  $\text{GdCu}_4\text{In}$  [16]. In addition, the neutron diffraction experiments have revealed that Ho moments in  $\text{HoCu}_4\text{Cd}$  are fully ordered [15] and Gd moments in  $\text{GdCu}_4\text{In}$  are partially ordered [16]. It is expected that the similar  $S_m$  value of  $\text{GdNi}_4\text{Cd}$  with that of  $\text{GdCu}_4\text{Cd}$  may indicate that Gd moments in  $\text{GdNi}_4\text{Cd}$  are also fully ordered without magnetic frustration. Note that the zero field  $C_m$  of  $\text{GdNi}_4\text{Cd}$  shows an unusual increase above 10 K, despite CEF splitting not being expected in Gd-based compounds. The full recovery of  $R \ln(8)$  entropy at  $T_N$  for  $\text{GdNi}_4\text{Cd}$  suggests that the broad feature above 10 K observed in  $C_m$  is due to the subtraction error.

#### IV. DISCUSSION

The RKKY exchange mechanism is examined for its relevance to  $T_N$  and  $\theta_p$  of  $RT_4X$  compounds. In this family, the  $4f$  moments of heavy rare earths are well respected with their Hund's rule ground-state  $J$  values, and their magnetic susceptibility curves are weakly affected by crystalline electric field (CEF) effects due to the small energy level splittings. In general, the strength of the molecular field  $\lambda$  can be estimated from Curie-Weiss temperature  $\theta_p$ . When  $\theta_p$  is positive, it indicates ferromagnetic (FM) interactions, while negative values indicate antiferromagnetic (AFM) interactions [17,18]. The magnetic ordering temperature ( $T_m$ ) reflects the exchange energy, which depends on the arrangement of magnetic moments on the lattice and the types of exchange interactions such as superexchange and RKKY interactions. In highly localized  $4f$  moment materials, it is often observed that  $T_c \sim \theta_p$  for ferromagnets and  $T_N < \theta_p$  for antiferromagnets, due to the simplified molecular field interactions. In some cases,

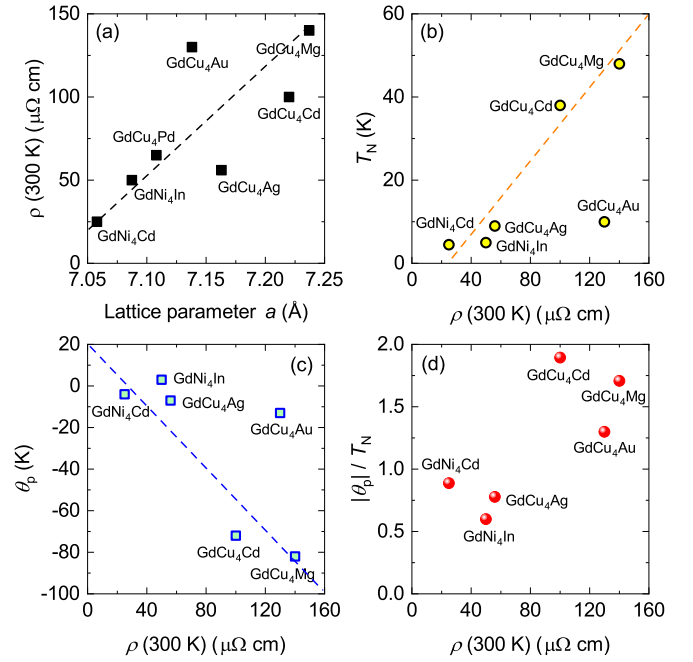


FIG. 8. Lattice parameter,  $\rho(300 \text{ K})$ ,  $T_N$ , and  $\theta_p$  of metallic  $\text{GdT}_4\text{X}$  compounds. (a)  $\rho(300 \text{ K})$  vs lattice parameter. (b)  $T_N$  vs  $\rho(300 \text{ K})$ . (c)  $\theta_p$  vs  $\rho(300 \text{ K})$ . (d)  $|\theta_p|/T_N$  vs  $\rho(300 \text{ K})$ .  $\rho(300 \text{ K})$ ,  $\theta_p$ , and  $T_N$  data are obtained from Ref. [19]. Dashed lines are guides to the eye.

$T_N$  can be further reduced by geometrically frustrated lattice structures such as fcc, kagome, and pyrochlore. Comparing  $\theta_p$  in this family can provide valuable insights into the relative strength of the exchange interactions and the dominant parameters affecting the magnitude of both  $\theta_p$  and  $T_m$  in isostructural settings. In particular, Gd-based compounds are suitable for this analysis because of the  $L = 0$  state.

For  $\text{GdT}_4\text{X}$  compounds, we investigate a correlation between the electrical resistivity at 300 K,  $\rho(300\text{K})$ , and other parameters such as the lattice parameter,  $T_N$ , and  $\theta_p$ .  $\rho(300 \text{ K})$  for metallic  $\text{GdT}_4\text{X}$  compounds is plotted in Fig. 8(a) against their lattice parameter. Note that  $\text{GdCu}_4\text{In}$  is not plotted in the figure, where the resistivity value of the semimetallic  $\text{RCu}_4\text{In}$  series is much larger than that of other metallic compounds in this family [3]. As the lattice parameter increases, the value of  $\rho(300 \text{ K})$  increases. This relationship has been observed in the  $\text{RCu}_4\text{In}$  and  $\text{RCu}_4\text{Cd}$  series, where a larger  $R$  results in a significant increase in resistivity values [3,20]. However, when  $R$  is varied from Gd to Tm in the  $\text{RNi}_4\text{Cd}$  series, the resistivity value at 300 K does not show a significant change (Fig. 5), despite the series exhibiting a similar degree of lattice contraction.

In a simple model, the electrical resistivity value is inversely proportional to the carrier density  $n$ , which is proportional to the density of states  $N(E_F)$  at the Fermi level. Therefore, variations of  $\rho(300 \text{ K})$  can be used as an approximation for the relative change in  $N(E_F)$  within this family of materials. Among this group,  $\text{GdNi}_4\text{Cd}$  exhibits the smallest resistivity value at 300 K,  $\rho(300 \text{ K}) \sim 25 \mu\Omega \text{ cm}$ , implying the largest  $N(E_F)$ . This result is supported by the observed values of electronic specific heat coefficient  $\gamma$  and

susceptibility  $\chi_0$  in nonmagnetic compounds, as  $\gamma$  and  $\chi_0$  values are proportional to  $N(E_F)$ . The  $\gamma$  and  $\chi_0$  values are 14 mJ/(mol K<sup>2</sup>) and  $1 \times 10^{-3}$  emu/mol for YNi<sub>4</sub>Cd [11] and 2.91 mJ/(mol K<sup>2</sup>) [3] and  $2.7 \times 10^{-5}$  emu/mol [21] for LuCu<sub>4</sub>In, respectively. YNi<sub>4</sub>Cd has the highest known  $\chi_0$  value among previously reported nonmagnetic  $RT_4X$  compounds. Thus, YNi<sub>4</sub>Cd is considered a good metal with  $\rho(300\text{ K}) \sim 10\ \mu\Omega\text{ cm}$ , while LuCu<sub>4</sub>In is a low-carrier-density semimetal with a very large  $\rho(300\text{ K}) \sim 1000\ \mu\Omega\text{ cm}$ .

The  $T_N$  and  $\theta_p$  values of the metallic  $GdT_4X$  compounds are displayed in Figs. 8(b) and 8(c), respectively, as a function of  $\rho(300\text{ K})$ . It appears that both  $T_N$  and  $\theta_p$  are approximately proportional to  $\rho(300\text{ K})$ . For metallic  $GdT_4X$ , the frustration parameter range is  $0.5 < f < 2$ , as shown in Fig. 8(d). Compounds with large  $|\theta_p|$ , such as GdCu<sub>4</sub>Cd and GdCu<sub>4</sub>Mg, tend to have the frustration parameter between 1 and 2, while compounds with small  $|\theta_p|$ , such as GdNi<sub>4</sub>Cd, GdNi<sub>4</sub>In, and GdCu<sub>4</sub>Ag, tend to have the frustration parameter less than 1. It has to be noted that the small value of  $f$  implies no magnetic frustration in metallic  $RT_4X$  compounds. The observed  $f$  suggests a variation in the strength of the RKKY interaction between the various Gd-Gd pairs responsible for  $T_N$  and  $\theta_p$ . It seems that the lattice parameter plays a significant role in tuning  $N(E_F)$  and  $T_N$  and  $\theta_p$  for metallic  $GdT_4X$  compounds.

It has been generally considered that the magnetic ordering temperature of  $4f$ -based metallic systems is proportional to the square of the effective exchange interaction ( $j_{sf}^2$ ) and  $N(E_F)$  [3]:  $T_N \propto j_{sf}^2 N(E_F)$ . However, the metallic  $GdT_4X$  compounds seem to follow the opposite direction where the larger  $N(E_F)$  does not necessarily enhance  $T_N$ . According to Ref. [22], the variation and sign change of  $\theta_p$  in Gd-based compounds can be explained by the RKKY mechanism. In the RKKY picture [13,23],  $\theta_p$  for both AFM and FM interactions can be expressed by

$$\theta_p = \frac{2(g-1)^2 J(J+1) \mathcal{J}(\mathbf{Q}=0)}{3k_B}, \quad (1)$$

$$\mathcal{J}(\mathbf{Q}=0) = -\frac{9\pi n_0^2}{4k_B E_F} j_{sf}^2 \sum_i F(2k_F R_i), \quad (2)$$

where  $\mathcal{J}(\mathbf{Q})$  is the effective exchange interaction between  $f$ -electron spins mediated by conduction electrons,  $(g-1)^2 J(J+1)$  is the de Gennes factor (dG) for the angular momentum quantum number  $J$ , and  $n_0$  is the average number of conduction electrons per unit cell. The RKKY sum varies between positive and negative values depending on a dimensionless quantity  $k_F R_i$ , leading to sign changes in  $\theta_p$ . Hence, the observed behavior can be explained by considering the position and direction of the RKKY sum, where the increment of  $k_F R_i$  leads to either an approach to or a departure from zero.

For  $RCu_4X$  ( $X = \text{Cd, In, Pd, Ag, and Au}$ ), the RKKY sum has been calculated assuming  $R$  and  $\text{Cu}$  atoms contribute three and one electron to the conduction band, respectively [3,6,22,24]. When the magnitude of  $\theta_p$  is large, this picture qualitatively explains the variation of  $\theta_p$ , with  $\theta_p$  linearly scaling with dG. However, when the  $\theta_p$  value is small and located near a sign change in the RKKY sum, the dG scaling breaks down. This has been observed for  $RCu_4X$  ( $X = \text{Ag and Au}$ ) and  $RNi_4\text{Cd}$ . For  $RCu_4X$  ( $X = \text{Ag and Au}$ ),  $\theta_p$  even shows a sign change when  $R$  is varied from Gd (dG = 15.8)

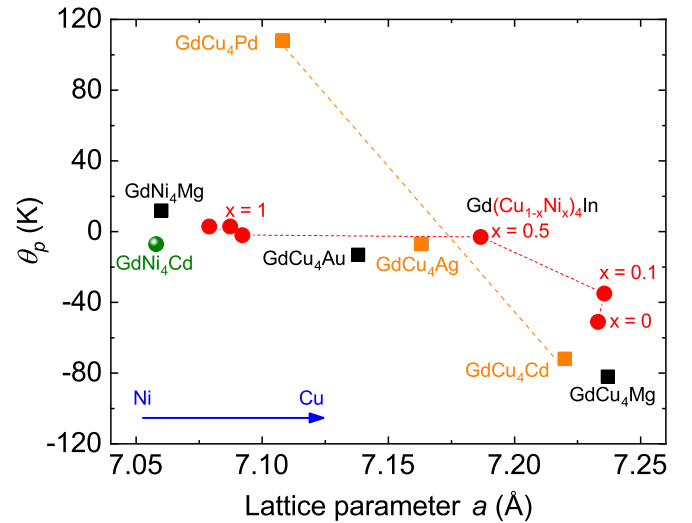


FIG. 9.  $\theta_p$  of  $GdT_4X$  compounds as a function of lattice parameter, obtained from Refs. [10] and [19]. Dotted and dashed lines are guides to the eye.

to Tm (dG = 1.2), which should not occur in the conventional RKKY mechanism. Therefore, constant conduction electrons or exchange interactions  $j_{sf}$  upon isoelectric substitution, assumed in the simple RKKY interaction, cannot be applied to real materials. Proper band structures must be considered to evaluate  $\mathcal{J}(\mathbf{Q})$ .

The observed  $\theta_p$  values of isostructural  $GdT_4X$  compounds are strongly dependent on the lattice parameter, implying a correlation with the interatomic spacing between the Gd ions. This relationship is demonstrated in Fig. 9, which plots  $\theta_p$  as a function of their lattice parameters. Since the nearest-neighbor Gd-Gd distance in this crystal structure is  $a/\sqrt{2}$ , the variation of  $\theta_p$  as a function of Gd-Gd distance is essentially the same as that shown in the figure. As seen in the figure, a decrease in the lattice parameter (i.e., a shorter Gd-Gd distance) leads to a shift of  $\theta_p$  toward a positive direction. Note that for other rare-earth elements ( $R = \text{Tb-Tm}$ ) that the lattice parameter of  $RT_4X$  closely follows the lanthanide contraction, regardless of  $R$ ,  $T$ , and  $X$ , and  $\theta_p$  indicates a similar trend as shown in Fig. 1.

We observe that the substitution of  $T$  and  $X$  in  $GdT_4X$  has two main effects: (i) a lattice effect due to the substitution of ions with different ionic sizes and (ii) an electronic effect due to the substitution of ions with different valence electrons [25]. Although the complete band structures are necessary to know the exact relationship between these two factors, we infer the dominant effect for the given substitutions from the experimental observations. Figure 8(a) suggests that the lattice contraction has a tendency to increase  $k_F$ , as  $\rho(300\text{ K})$  is proportional to  $1/N(E_F) \propto 1/k_F$ . For the isoelectric substitution of Ag with Au in  $GdCu_4X$ , the change in  $\theta_p$  is small due to the small lattice contraction. Similarly, substituting Cd with Mg in  $GdCu_4X$  results in insignificant variations of  $\theta_p$ , possibly due to the negligible increase in  $N(E_F)$  resulting from the small lattice expansion.

For  $X = \text{Cd} \rightarrow \text{Ag} \rightarrow \text{Pd}$  substitution, both the lattice and electronic effects are needed to be considered. Since the exact

number of valence electrons contributing to the conduction band is unknown, we simply consider the electronic configurations of  $X$  atoms in  $\text{GdCu}_4X$  ( $X = \text{In, Cd, Ag, Pd}$ ): the outer electrons are progressively removed from  $[\text{Kr}]4d^{10}5s^25p^1$  in In, followed by  $[\text{Kr}]4d^{10}5s^2$  in Cd,  $[\text{Kr}]4d^{10}5s^1$  in Ag, and  $[\text{Kr}]4d^{10}$  in Pd. Note that Au has the electronic configuration of  $[\text{Kr}]5d^{10}6s^1$ , which is similar to Ag but with a higher energy level. Ag has one less  $5s$  electron than Cd, contributing one less electron to the conduction band and decreasing  $k_F$ . When  $X$  is varied from Cd to Ag,  $\theta_p$  shows a very large jump from  $-78$  to  $-7$  K, suggesting a large electronic effect. When  $X$  is substituted from Ag to Pd,  $\theta_p$  changes from  $-7$  to  $+108$  K. The degree of lattice contraction in the Ag  $\rightarrow$  Pd substitution is similar to that in the Cd  $\rightarrow$  Ag substitution, implying the electronic effect has a greater impact on  $\theta_p$  than the lattice effect. The removal of the outermost electrons in the  $s$  orbital in  $\text{GdCu}_4X$  (Cd, Ag, Pd) makes the compound more ferromagnetic, as indicated by the sign change of  $\theta_p$ . A similar transition from a strong AFM to strong FM exchange interactions between Gd moments has been observed in Gd monopnictides  $\text{GdX}_p$  ( $X_p = \text{Bi, Sb, As, P, and N}$ ), which also form the fcc lattice by Gd moments. For  $\text{GdX}_p$ , the lattice parameter plays a crucial role in controlling  $\theta_p$  [26–28]. When  $X_p$  is changed from Bi to N, which is an isoelectric substitution, the  $\theta_p$  values change from  $-45$  to  $+81$  K as the lattice parameter decreases by 20%. The lattice contraction for  $\text{GdX}_p$  is much larger than that for the  $\text{GdCu}_4X$  case ( $-1.5\%$ ). For  $\text{GdX}_p$ , the  $J_1$  and  $J_2$  model explains this transition, as the strong distance-dependent  $d-f$  mixing interactions result in a strong FM  $J_1$  and weak AFM  $J_2$  via lattice contraction [27,29].

For the case of In  $\rightarrow$  Cd substitution, the trend is reversed in  $\text{GdCu}_4X$ . When an electron from the  $5p$  orbital of In is removed, contributing one less electron to the conduction band, the  $\theta_p$  value is expected to be decreased by reduced  $k_F$ . However,  $\theta_p$  becomes more AFM as  $X$  changes from In to Cd. The same behavior is also observed in  $\text{GdNi}_4X$ . The In  $\rightarrow$  Cd substitution involves  $p$ -orbital electrons contributing to the Fermi level, while the Cd  $\rightarrow$  Ag  $\rightarrow$  Pd substitution involves  $s$ -orbital electrons. It is plausible to conjecture that different types of electrons ( $s$ -like or  $p$ -like) have different effects on the conduction bands, leading to different exchange interactions. This observation suggests that the type of electrons contributing to the conduction band seems to determine  $\theta_p$ .

The  $T = \text{Cu} \rightarrow \text{Ni}$  substitution in  $\text{GdT}_4X$  has a relatively large lattice ( $\Delta a/a \sim -3\%$ ) contraction, and it is expected to cause a shift of  $\theta_p$  towards a large, positive value. However, the observed  $\theta_p$  values for all Ni-based compounds are small. The Cu atom in these families has a closed  $d$  shell with electronic configuration of  $[\text{Ar}]3d^{10}4s^1$ , which is confirmed from  $\text{YbCu}_4X$  by Cu  $K$ -edge x-ray absorption spectroscopy experiments, and provides an electron from its  $s$  orbital to the conduction band [30]. It has been suggested that Cu and Ni atoms provide the same number of  $s$  electrons to the conduction band [31]. Since Ni has one less  $d$  electron than Cu and there are four more Ni atoms than Gd and  $X$  atoms in the unit cell, the number of  $d$  electrons contributing to the conduction band should be considered. It seems that unlike the case for removing  $s$  electrons, reducing the number of  $d$  electrons

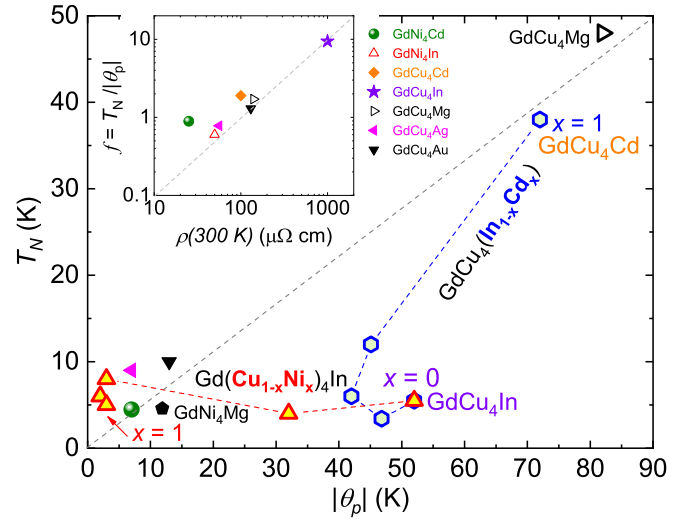


FIG. 10.  $T_N$  as a function of  $|\theta_p|$ , obtained from Ref. [19]. Inset: The frustration parameter  $f = |\theta_p|/T_N$  as a function of room-temperature resistivity  $\rho(300 \text{ K})$ .  $\rho(300 \text{ K})$  of  $\text{GdCu}_4\text{In}$  (purple star) is taken from Ref. [3]. Dotted and dashed lines are guides to the eye.

does not induce a drastic change of  $\theta_p$  from large negative to large positive. This may be partly due to the electronic effect being partially offset by the lattice effect. Again, the type of electrons,  $d$  vs  $s$ , seems to be important to describe actual materials with the RKKY interaction.

We now examine how the observed  $T_N$  values for  $\text{GdT}_4X$  vary in relation to  $\theta_p$  and carrier density upon substitution in  $T$  and  $X$ . In metallic  $\text{RT}_4X$ , the magnetic ordering temperature exhibits a strong correlation with  $\theta_p$ ; higher  $\theta_p$  values result in higher  $T_N$  values, as shown in Fig. 10. In antiferromagnets, the ordered state is characterized by a nonzero wave vector  $\mathbf{Q}$ , where the magnetic ordering temperature is given by the equation  $T_m = 2(g-1)^2 J(J+1) \mathcal{J}(\mathbf{Q}) / 3k_B$ . Thus, it has often been observed that  $T_N$  is lower than  $|\theta_p|$ . Additionally,  $T_N < |\theta_p|$  may be a sign of magnetic frustration. Note that the wave vector in ferromagnets is zero,  $\mathbf{Q} = 0$ , in the ordered state. The small  $f$  values ranging from 0.5 to 2 in metallic  $\text{RT}_4X$  suggest that the effect of the magnetic frustration is absent. Thus, the wave-vector-dependent exchange interaction is responsible for  $T_N < |\theta_p|$  in metallic  $\text{RT}_4X$  compounds. However, the large value of  $f \sim 10$  observed in the  $\text{GdCu}_4\text{In}$  case implies the magnetic frustration in a low-carrier-density, semimetallic state which results from the Fermi level lying on the quasigap in the density of states [32]. It has been suggested that the magnetic frustration in Gd moments arises from short-range superexchange interactions due to the insufficient carrier density, which prevents the formation of a long-range magnetic order. [3,16].

In the  $J_1 - J_2$  model, the relative strength between nearest-neighbor exchange interaction  $J_1$  and next-nearest-neighbor exchange interaction  $J_2$  gives rise to various magnetic structures in the fcc antiferromagnets, including type I ( $\alpha = J_2/J_1 \leq 0$ ), type II ( $1/2 \leq \alpha \leq \infty$ ), and type III ( $0 \leq \alpha \leq 0.5$ ) [33,34]. For the low-carrier-density systems, neutron diffraction experiments have confirmed that the magnetic structure of  $\text{GdCu}_4\text{In}$  and  $\text{HoCu}_4\text{In}$  is partially frustrated,

where half of the rare-earth moments are frustrated and the other half are ordered below  $T_N$  [15,16]. This magnetic structure is intermediate between type I and type III, and is realized only when  $J_2$  is zero. We suspect that the absence of  $J_2$  may result from the low-carrier-density nature. Neutron diffraction experiments for the metallic case has shown that  $\text{HoCu}_4\text{Cd}$  has a type-II magnetic structure. It is not unreasonable to assume that  $\text{GdCu}_4\text{Cd}$  has the same type-II magnetic structure. In this assumption, as the concentration of Cd in  $\text{GdCu}_4(\text{In}_{1-x}\text{Cd}_x)$  increases, the magnetic structure is expected to evolve from the partially frustrated to type II. With this substitution, the lattice parameter changes a little, leading to a small change in  $\theta_p$ . In contrast, there is a significant enhancement of  $T_N$  likely due to a significant increase in the carrier density and, consequently, greater contribution from  $J_2$ . Although the carrier density is significantly increased,  $T_N$  remains near 5 K for the  $\text{Gd}(\text{Cu}_{1-x}\text{Ni}_x)_4\text{In}$  case. Increasing  $x$  in  $\text{Gd}(\text{Cu}_{1-x}\text{Ni}_x)_4\text{In}$  causes a large variation of  $\theta_p$  due to a large change of the lattice parameter. Although the recovered metallic carrier density induces a long-range RKKY interaction,  $T_N$  cannot exceed  $|\theta_p|$  because it is bound by  $|\theta_p|$ . In these substitutions, the doping concentration  $x$  does not result in a continuous variation of  $\theta_p$ , where  $\theta_p$  changes abruptly at the critical concentration [3,9]. A similar behavior has been observed from the carrier density dependence of  $\theta_p$  in semiconductors [35,36]. The steplike change of  $\theta_p$  requires a modified RKKY model with a two-valence-band approximation and a finite mean free path for carriers [36]. Thus, more realistic models are necessary to explain the variation of  $\theta_p$  in  $\text{GdT}_4\text{X}$ .

The observation of small  $T_N$  values in  $\text{GdNi}_4\text{X}$  is not surprising because  $T_N$  is bounded by  $|\theta_p|$ . However, it is worth investigating what makes  $\theta_p$  of Ni-based compounds small. According to the calculation of  $\mathcal{J}(\mathbf{Q})$  for a fcc lattice [22], various magnetic structures are possible depending on  $k_F$ . The calculation shows that the FM structure is stabilized at low  $k_F$  and transitions into the type-II AFM structure as  $k_F$  increases. For  $\text{GdCu}_4\text{X}$  ( $X = \text{Cd}, \text{Ag}, \text{and Pd}$ ) cases, the variation of  $\theta_p$  from a large negative to large positive may be related to

the FM–AFM transition region in the  $\mathcal{J}(\mathbf{Q})$  calculation. We conjecture for  $\text{GdNi}_4\text{X}$  ( $X = \text{Cd}, \text{Mg}, \text{and In}$ ) cases that the strength of the exchange interactions between molecular fields produced by rare-earth planes ( $\theta_p$ ) is suppressed by lattice contraction. Further electronic band structure calculations are necessary to determine the potential connection between the incomplete  $d$  shell of Ni and the lack of strong ferromagnetism in  $\text{GdNi}_4\text{X}$ .

## V. SUMMARY

We have successfully grown single crystals of  $\text{RNi}_4\text{Cd}$  ( $R = \text{Y}, \text{Ce}, \text{Nd}, \text{Sm}, \text{and Gd–Tm}$ ), confirmed all samples to crystallize into the  $\text{MgCu}_4\text{Sn}$ -type structure, and characterized their physical properties. Ce and Ni ions are nonmagnetic, with Ce being a 4+ valence state. The other magnetic rare-earth ions are in a 3+ valence state, and the magnetic behavior of these heavy rare-earth compounds is well described by Hund’s rule ground state  $J$ . We observed that the Curie-Weiss temperature  $\theta_p$  of isostructural compounds  $\text{RT}_4\text{X}$  ( $R = \text{Gd–Tm}$ ,  $T = \text{Cu and Ni}$ , and  $X = \text{Cd}, \text{In}, \text{Mg}, \text{Ag}, \text{and Au}$ ) changes towards a positive direction as the lattice parameter decreases, except for  $\text{RCu}_4\text{Pd}$ . This behavior can be qualitatively explained by RKKY theory. We have also investigated the parameters and conditions affecting  $\theta_p$  and  $T_N$  in  $\text{GdT}_4\text{X}$ . The substitution of  $T$  and  $X$  in  $\text{GdT}_4\text{X}$  has both lattice and electronic effects, with the dominant effect deduced from experimental observations. Lattice contraction tends to increase  $k_F$ , while removing the outermost electrons in the  $s$  orbital in  $\text{GdCu}_4\text{X}$  results in a stronger ferromagnetic interaction. In contrast,  $\theta_p$  of  $\text{GdNi}_4\text{X}$  compounds approaches zero as the lattice parameter decreases. Further investigation is necessary to understand this relationship to  $\theta_p$  and  $T_N$ .

## ACKNOWLEDGMENTS

This work was supported by the Canada Research Chairs, Natural Sciences and Engineering Research Council of Canada, and Canada Foundation for Innovation program.

- 
- [1] F. Tappe, C. Schwickert, and R. Pöttgen, Ternary ordered Laves phases  $\text{RENi}_4\text{Cd}$ , *Intermetallics* **24**, 33 (2012).
- [2] S. Linsinger, M. Eul, C. Schwickert, R. Decourt, B. Chevalier, U. C. Rodewald, J. L. Bobet, and R. Pöttgen, Structure, homogeneity ranges, magnetic, and electrical properties of the ordered Laves phases  $\text{RENi}_4\text{Mg}$  with  $\text{MgCu}_4\text{Sn}$  type structure, *Intermetallics* **19**, 1579 (2011).
- [3] V. Fritsch, J. D. Thompson, J. L. Sarrao, H.-A. Krug von Nidda, R. M. Eremina, and A. Loidl, Correlation between magnetic frustration and electrical conductivity in  $\text{RInCu}_4$  compounds ( $R = \text{Gd–Tm}$ ), *Phys. Rev. B* **73**, 094413 (2006).
- [4] S. Stein, L. Heletta, T. Block, and R. Pöttgen, Rare earth-copper-magnesium intermetallics: Crystal structure of  $\text{Ce–CuMg}$ , magnetocaloric effect of  $\text{GdCuMg}$  and physical properties of the Laves phases  $\text{RECu}_4\text{Mg}$  ( $\text{RE} = \text{Sm}, \text{Gd}, \text{Tb}, \text{Tm}$ ), *Z. Naturforsch. B* **73**, 987 (2018).
- [5] S. Abe, H. Nakazawa, T. Kaneko, H. Yoshida, K. Kamigaki, Y. Nakagawa, and S. Miura, Magnetic properties of cubic intermetallic compounds  $\text{RCu}_4\text{Pd}$  ( $R = \text{Gd}, \text{Tb}, \text{Dy}, \text{Ho and Er}$ ), *J. Phys. Soc. Jpn.* **58**, 3328 (1989).
- [6] T. Takeshita, S. K. Malik, A. A. ElAttar, and W. E. Wallace, Crystal structure and magnetic properties of  $\text{RCu}_4\text{Ag}$  ( $R = \text{Rare Earth}$ ) intermetallic compounds, *AIP Conf. Proc.* **34**, 230 (1976).
- [7] T. Kaneko, S. Arai, S. Abe, and K. Kamigaki, Magnetic properties of cubic  $\text{RAuCu}_4$  ( $R = \text{Gd}, \text{Tb}, \text{Dy}, \text{Ho and Er}$ ) intermetallic compounds, *J. Phys. Soc. Jpn.* **55**, 4441 (1986).
- [8] V. Fritsch, J. D. Thompson, and J. L. Sarrao, Spin and orbital frustration in  $\text{RInCu}_4$  ( $R = \text{Gd}, \text{Dy}, \text{Ho}, \text{and Er}$ ), *Phys. Rev. B* **71**, 132401 (2005).
- [9] S. G. Mercena, E. C. Mendona, C. T. Meneses, L. S. Silva, J. G. S. Duque, C. B. R. Jesus, J. C. Souza, and P. G. Pagliuso, Complex magnetic behavior along the  $\text{GdIn}(\text{Ni}_x\text{Cu}_{1-x})_4$  ( $0.00 \leq x \leq 1.00$ ) series of compounds, *J. Appl. Phys.* **125**, 063903 (2019).



- [10] The lattice parameter and Curie-Weiss temperature are taken from previous reports:  $\text{GdNi}_4\text{Cd}$  (polycrystalline) [1],  $\text{RNi}_4\text{Mg}$  [2],  $\text{RCu}_4\text{Cd}$  [3],  $\text{RCu}_4\text{In}$  [8],  $\text{RCu}_4\text{Mg}$  [4],  $\text{RCu}_4\text{Pd}$  [5],  $\text{RCu}_4\text{Ag}$  [6], and  $\text{RCu}_4\text{Au}$  [7].
- [11] J. Lee, H. Park, N. R. Lee-Hone, D. M. Broun, and E. Mun, Thermodynamic and transport properties of  $\text{YbNi}_4\text{Cd}$ , *Phys. Rev. B* **97**, 195144 (2018).
- [12] K. Kadir, D. Noreus, and I. Yamashita, Structural determination of  $\text{AMgNi}_4$  (where  $A = \text{Ca, La, Ce, Pr, Nd}$  and  $\text{Y}$ ) in the  $\text{AuBe}_5$  type structure, *J. Alloys Compd.* **345**, 140 (2002).
- [13] P. G. De Gennes, Indirect interactions between 4f shells in rare earth metals, *J. phys. Radium* **23**, 510 (1962).
- [14] M. Bouvier, P. Lethuillier, and D. Schmitt, Specific heat in some gadolinium compounds. I. Experimental, *Phys. Rev. B* **43**, 13137 (1991).
- [15] O. Stockert, J. U. Hoffmann, M. Mühlbauer, A. Senyshyn, M. M. Kozá, A. A. Tsirlin, F. M. Wolf, S. Bachus, P. Gegenwart, R. Movshovich, S. Bobev, and V. Fritsch, Magnetic frustration in a metallic fcc lattice, *Phys. Rev. Res.* **2**, 013183 (2020).
- [16] H. Nakamura, N. Kim, M. Shiga, R. Kmiec, K. Tomala, E. Ressouche, J. P. Sanchez, and B. Malaman, The partially disordered state of the frustrated face-centred cubic antiferromagnet  $\text{GdInCu}_4$ , *J. Condens. Matter Phys.* **11**, 1095 (1999).
- [17] J. S. Smart, *Effective Field Theories of Magnetism* (Saunders, Philadelphia, 1966).
- [18] S. Mugiraneza and A. M. Hallas, Tutorial: A beginner's guide to interpreting magnetic susceptibility data with the Curie-Weiss law, *Commun. Phys.* **5**, 95 (2022).
- [19] The  $\rho(300\text{ K})$  values are taken from the following:  $\text{GdNi}_4\text{Cd}$  (this work),  $\text{GdCu}_4\text{Cd}$  [3],  $\text{GdCu}_4\text{In}$  [3],  $\text{GdCu}_4\text{Pd}$  [38], and  $\text{GdCu}_4\text{Au}$  [39]. Because  $\rho(300\text{ K})$  data for some Gd-based compounds are not available,  $\rho(300\text{ K})$  is inferred from its analog compound that differs by only  $R$ :  $\text{GdNi}_4\text{In}$  averaged  $\rho(300\text{ K})$  value of  $\text{YbNi}_4\text{In}$  and  $\text{NdNi}_4\text{In}$  [37];  $\text{GdCu}_4\text{Mg}$  obtained from  $\text{SmCu}_4\text{Mg}$  [4];  $\text{GdCu}_4\text{Ag}$  obtained from  $\text{NdCu}_4\text{Ag}$  [40].  $T_N$  and  $\theta_p$  are taken from the following:  $\text{GdNi}_4\text{Cd}$  (this work),  $\text{GdNi}_4\text{Mg}$  [2],  $\text{GdCu}_4\text{Mg}$  [4],  $\text{GdCu}_4\text{Pd}$  [5],  $\text{GdCu}_4\text{Ag}$  [6],  $\text{GdCu}_4\text{Au}$  [7],  $\text{GdCu}_4(\text{In}_{1-x}\text{Cd}_x)$  [3], and  $\text{Gd}(\text{Cu}_{1-x}\text{Ni}_x)_4\text{In}$  [9].
- [20] H. Nakamura, A. Uenishi, K. Ito, M. Shiga, T. Kuwai, and J. Sakurai, Transport properties of  $\text{RInCu}_4$  with C15b-type structure, *J. Magn. Magn. Mater.* **140**, 923 (1995).
- [21] P. G. Pagliuso, C. Rettori, S. B. Oseroff, J. Sarrao, Z. Fisk, A. Cornelius, and M. F. Hundley, ESR of  $\text{Gd}^{3+}$  in  $\text{LuInCu}_4$  intermetallic compound, *Solid State Commun.* **104**, 223 (1997).
- [22] J. Sakurai, Y. Kubo, T. Kondo, J. Pierre, and E. F. Bertaut, Relations between the Ruderman-Kittel-Kasuya-Yosida interaction electron concentration and crystal structure, *J. Phys. Chem. Solids* **34**, 1305 (1973).
- [23] M. A. Ruderman and C. Kittel, Indirect exchange coupling of nuclear magnetic moments by conduction electrons, *Phys. Rev.* **96**, 99 (1954); T. Kasuya, A theory of metallic ferro- and antiferromagnetism on zener's model, *Prog. Theor. Phys.* **16**, 45 (1956); K. Yosida, Magnetic properties of Cu-Mn alloys, *Phys. Rev.* **106**, 893 (1957).
- [24] S. Abe, Y. Atsumi, T. Kaneko, and H. Yoshida, Magnetic properties of  $\text{RCu}_4\text{In}$  ( $R = \text{Gd-Er}$ ) intermetallic compounds, *J. Magn. Magn. Mater.* **104-107**, 1397 (1992).
- [25] P. Monachesi and A. Continenza, Electronic and volumetric effects in ternary compounds of ytterbium, *Phys. Rev. B* **54**, 13558 (1996).
- [26] T. R. McGuire, R. J. Gambino, S. J. Pickart, and H. A. Alperin, Magnetic structure and exchange interactions in cubic gadolinium compounds, *J. Appl. Phys.* **40**, 1009 (1969).
- [27] D. X. Li, Y. Haga, H. Shida, T. Suzuki, Y. S. Kwon, and G. Kido, Magnetic properties of stoichiometric Gd monopnictides, *J. Phys.: Condens. Matter* **9**, 10777 (1997).
- [28] C. G. Duan, R. F. Sabiryanov, W. N. Mei, P. A. Dowben, S. S. Jaswal, and E. Y. Tsymlal, Magnetic ordering in Gd monopnictides: Indirect exchange versus superexchange interaction, *Appl. Phys. Lett.* **88**, 182505 (2006).
- [29] T. Kasuya and D. X. Li, Mechanism of strong ferromagnetism in  $\text{GdN}$ , *J. Magn. Magn. Mater.* **167**, L1 (1997); Anomalous exchange mechanism in Gd monopnictides, *Phys. B: Condens. Matter* **230-232**, 472 (1997).
- [30] H. Anzai, S. Ishihara, H. Shiono, K. Morikawa, T. Iwazumi, H. Sato, T. Zhuang, K. T. Matsumoto, and K. Hiraoka, Mixed-valence state of the rare-earth compounds  $\text{YbXCu}_4$  ( $X = \text{Mg, Cd, In, and Sn}$ ): Magnetic susceptibility, x-ray diffraction, and x-ray absorption spectroscopy investigations, *Phys. Rev. B* **100**, 245124 (2019).
- [31] P. G. Pagliuso, C. Rettori, J. L. Sarrao, A. Cornelius, M. F. Hundley, Z. Fisk, and S. B. Oseroff, Electron spin resonance of  $\text{Gd}^{3+}$  and  $\text{Nd}^{3+}$  in  $\text{LuInA}_4$  ( $A = \text{Cu, Ni}$ ), *Phys. Rev. B* **60**, 13515 (1999).
- [32] E. Figueroa, J. M. Lawrence, J. L. Sarrao, Z. Fisk, M. F. Hundley, and J. D. Thompson, Hall effect in  $\text{YbXCu}_4$  and the role of carrier density in the  $\text{YbInCu}_4$  valence transition, *Solid State Commun.* **106**, 347 (1998).
- [33] N. N. Sun and H. Y. Wang, The  $J_1 - J_2$  model on the face-centered-cubic lattices, *J. Magn. Magn. Mater.* **454**, 176 (2018).
- [34] M. E. Lines, Antiferromagnetism in the face-centered cubic lattice. I. The random-phase green's function approximation, *Phys. Rev.* **139**, A1304 (1965).
- [35] T. Story, G. Karczewski, L. Świerkowski, and R. R. Galazka, Magnetism and band structure of the semimagnetic semiconductor  $\text{Pb-Sn-Mn-Te}$ , *Phys. Rev. B* **42**, 10477 (1990).
- [36] H. J. M. Swagten, W. J. M. de Jonge, R. R. Galazka, P. Warmenbol, and J. T. Devreese, Hole density and composition dependence of ferromagnetic ordering in  $\text{Pb-Sn-Mn-Te}$ , *Phys. Rev. B* **37**, 9907 (1988).
- [37] M. D. Koterlin, B. S. Morokhivskii, I. D. Shcherba, and Y. M. Kalychak, Transport and magnetic properties of the compounds  $\text{YbNi}_4\text{In}$  and  $\text{YbNiIn}_4$  with valence-unstable Yb, *Phys. Solid State* **41**, 1759 (1999).
- [38] S. Abe, H. Nakazawa, T. Kaneko, H. Yoshida, and K. Kamigaki, Magnetic and electric properties of intermetallic compounds  $\text{RCu}_4\text{Pd}$  ( $R = \text{Gd, Tb, Dy, Ho AND Er}$ ), *J. Phys. Colloq.* **49**, C8-385 (1988).
- [39] A. K. Bashir, M. B. T. Tchokonté, D. Britz, B. M. Sondezi, and A. M. Strydom, Magnetic and thermodynamic properties of  $\text{GdCu}_4\text{Au}$ , *J. Phys.: Conf. Ser.* **592**, 012050 (2015).
- [40] T. Tayama, Y. Takayama, Y. Miura, S. Zhang, and Y. Isikawa, Low-temperature magnetization of antiferromagnet  $\text{NdCu}_4\text{Ag}$ , *J. Phys. Soc. Jpn.* **80**, SA074 (2011).